We are IntechOpen,
the world's leading publisher of
Open Access books
Built by scientists, for scientists

4,800

Open access books available

122,000

International authors and editors

135M

Downloads

Our authors are among the

154

Countries delivered to

TOP 1%

most cited scientists

12.2%

Contributors from top 500 universities

CLARIVATE ANALYTICS
BOOK CITATION INDEX
INDEXED

WEB OF SCIENCE™

Selection of our books indexed in the Book Citation Index
in Web of Science™ Core Collection (BKCI)

Interested in publishing with us?
Contact book.department@intechopen.com

Numbers displayed above are based on latest data collected.
For more information visit www.intechopen.com

Bio-inspired Robotic Fish with Multiple Fins

Parasar Kodati and Xinyan Deng
University of Delaware
U.S.A.

1. Introduction

In order to improve the performance of AUVs in terms of efficiency and maneuverability, researchers have proposed biomimetic propulsion systems that swim using flapping fins rather than rotary propellers. This calls for the exploration of unique locomotion characteristics found in a variety of fish for use in underwater robots. (Sfakiotakis et. al., 1999) present a good review of fish swimming modes targeted at roboticists interested in aquatic locomotion. A classification scheme of fish locomotion mechanisms, originally presented in (Lindsey, 2006) and was modified in (Colgate & Lynch, 2004), is shown in Fig. 1. The three main swimming styles are characterized by undulatory body motion, undulatory fin motion, and oscillatory fin motion. A more traditional classification is one proposed by Breder (Breder, 1926) that broadly identifies two styles of swimming: one is Body and/or Caudal Fin (BCF) locomotion, and the other is Median and/or Paired Fin (BMP) locomotion. Fish classes that use varying degrees of body undulation and/or caudal fin oscillations for thrust generation are examples of BCF swimming, and fish that use paired fins like the left and right pectoral fins, dorsal, and ventral pelvic fins for thrust generation are classified under the MPF swimming style.
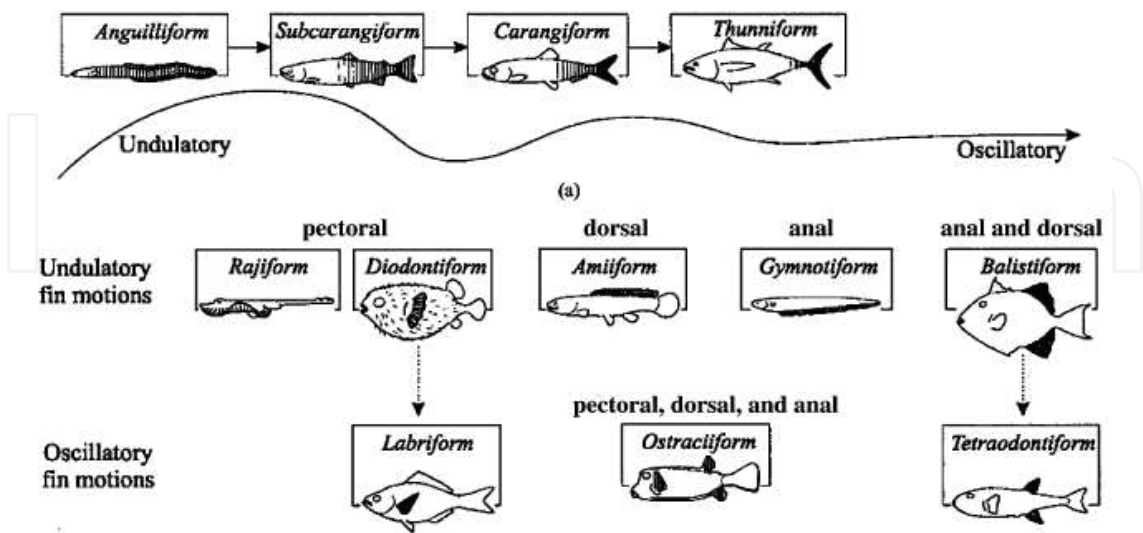

Fig. 1. Fish Classification based on swimming styles (Lindsey, 1978 & Colgate, 2004).

MIT's Robotuna marked the beginning of the biomimetic approach in underwater vehicles (Triantafyllou & Triantafullou, 1995). Barrett et. al. (Barrett, et. al, 1999) demonstrated that

the highly articulated robotic fish experienced less drag with undulatory motion than that seen without body undulation. Zhu (Zhu, et. al, 2002) also identified a vorticity control phenomenon, which explains the interaction of the vortices shed by the undulating body and the ones in the wake shed by the tail fin. Such interaction of the body with the wake was also shown to reduce the muscle activity in fish (Liao, et. al, 2003). Anguilliform requires a greater amount of body undulation and thus more degrees of freedom must be connected in series to form a robot. McIsaac and Ostrowski (McIsaac & ostrowski, 2003) studied motion planning and control of a serial chain robotic eel. They generated gaits (time functions of the joint angles) for the straight and turning motions of 3-link and 5-link robots. MacIver (MacIver, et. al, 2004) presented some aspects of underwater vehicle design in the areas of sensing and motion mechanisms of a knifefish in (Epstein, et. al, 2006).

The Biologically Inspired Robotics Group at EPFL presented a swimming and crawling robot, BoxyBot (Lachat, et. al, 2006) that is "loosely inspired by the boxfish". The focus there was to mimic boxfish-like switching of swimming modes under different speed ranges. More recent biologically inspired robot designs include Basilisk lizard like water running robot (Floyd, et. al, 2006).

Recently, a new class of biorobotic underwater vehicles based on the biomimetic principles of flapping foils are being designed. These platforms employ fin designs and motion kinematics that are the result of experimental and computational fluid mechanics work. Licht et. al. (Licht, et. al, 2004) presented the design of a vehicle platform with four heaving and pitching foils. A team of ocean engineers, fluid mechanists and biologists proposed a concept vehicle taking advantage of high efficiency foils in combination with articulated pectoral fins with rays for enhanced maneuverability (Fish, et. al, 2003). Pulsatile jet formation loosely inspired by squid is presented in (Mohseni, 2004). Kato's Bass III (Kato & Wicaksono, 2000) is the latest 3 DOF pectoral fin based vehicle designed for low speed precise maneuvering. Bandyopadhyay (Bandyopadhyay, 2005) presented a comprehensive review of approaches on various fronts of biomimetic underwater vehicle technology like high lift generating fin hydrodynamics, vehicle maneuverability using pectoral fins, muscle-like actuators and neuroscience based control.
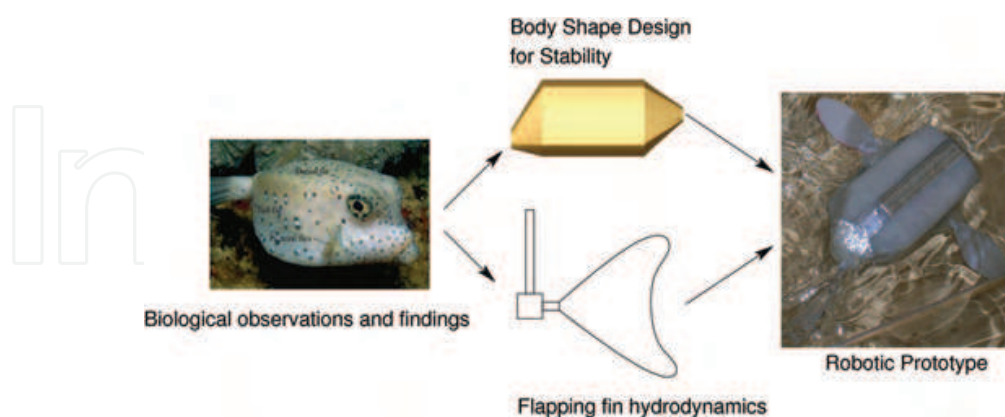

Fig. 2. Bio-inspired robotic fish with multiple fins.

Most Autonomous Underwater Vehicles (AUVs) today are larger ones applied extensively from environmental monitoring to oil and gas exploration (Yuh, 2000). However, these AUVs are not suitable for applications where the vehicle has to explore confined spaces like ship wrecks or oil pipe lines, where maneuverability and stability are more important than speed. Tasks such as these call for designs that are small, maneuverable and precisely

controlled. The work presented in this chapter is a step towards realizing such Micro Underwater Vehicles(MUVs). Here we present the research leading to the design and fabrication of a bio-inspired robotic fish with multiple fins for propulsion and control [Fig.2]. We present the experimental setup for studying flapping fin hydrodynamics and the force measurement results from flexible fins, and we presents the modeling of boxfish-like engineering shapes incorporating key morphological features that are responsible for self correcting vorticity generation as explained by Bartol et. al. in (Bartol, et. al, 2005).

2. Fin hydrodynamics

A robotic flapper was designed to generate fin motion in three independent rotational degrees of freedom, with a force/torque sensor attached to the base of the fin. The flapper was mounted on a linear stage that was driven a stepper motor. A larger tank was used to allow for linear motion. The tank was filled with refined paraffinic oil. This setup allows us to reply the fin kinematics while measuring instantaneous hydrodynamic forces.

The thrust (force in the direction of motion) produced by a flapping fin is a result of its interaction with the surrounding fluid. In the case of simple flapping (for example the caudal fin of a boxfish in cruise mode) this interaction can lead to lift and drag based forces as well as added mass effects (resulting from the deceleration of fluid set in motion by previous strokes). Fig. 3 shows such forces acting on a foil. The lift component (L) of the total force (F) is a result of periodic vortex shedding while the rest of the components are due to drag(D).
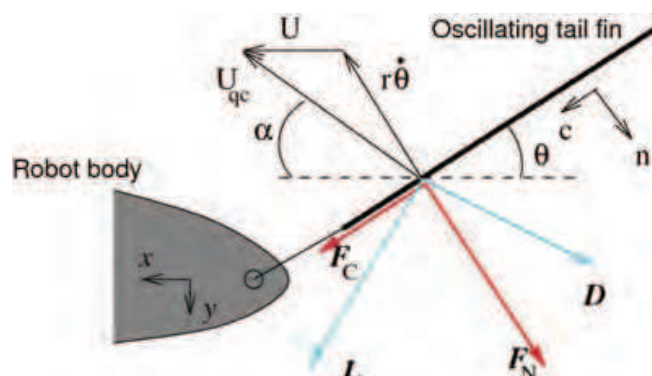

Fig. 3. Forces acting on an oscillating tail fin.

In this study, a boxfish like fin shape was used as the template to vary the fin geometry, therefore its flexibility. To change the chord wise flexibility, the dimensions c1 and c2 have been varied while fixing the aspect ratio and the total area of the fin. This kind of parametric variation displaces the center of pressure of the fin, thus varying the degree of flexing. Fig. 4 shows the shape template used to obtain different tail fin shapes by varying c1 and c2. Four shapes (labeled S1 to S4) from this continuum have been considered experimentally. Table 1 gives the geometric dimensions. The shapes were cut from 0.6mm thick Delrin, 0.1mm thick Polyimide, and 0.6mm thick Polyethylene in order to look at them over a range of material stiffness. In fact, from a flexibility point of view all twelve shapes (four profiles, three materials) form a continuum of flexural stiffness (EI) values, which have a strong correlation to the amount of flexing (Combes & Daniel, 2003). The term captures the elasticity (E, Young's modulus) of the fin material as well as the shape geometry (I, second moment of area) that together determine the fin's flexibility.
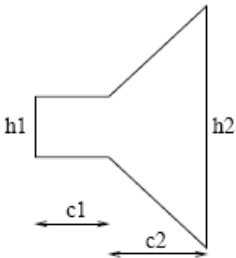
Fig. 4. Fin shape parameters.

Shape	C1 (cm)	C2 (cm)
S1	4.00	4.11
S2	3.01	4.57
S3	2.02	5.02
S4	1.00	5.50

Table 1. Four shapes studied.

Each shape/material combination (with the exception of shape S1 of Polyethylene) was flapped harmonically at frequencies ranging (in 0.1 Hz intervals) from 0.3Hz to 0.8 Hz, while being towed at a speed of 0.08 m/s. The Strouhal number is a non-dimensional number that relates the forward velocity, U to the flapping frequency,f as:

$$St = fw/U \qquad (1)$$

where w is the wake width. In our case, w was treated as the width of a single fin stroke.
We define the non-dimensional thrust and drag coefficients as

$$C_T = 2F_x/(\rho A U^2) \qquad (2)$$

$$C_D = 2F_y/(\rho A U^2) \qquad (3)$$

where F_x and F_y are forward thrust and side way components of the force vector in the horizontal plane, ρ is the density of the fluid and A is the fin area. η is defined as a measure of forward propulsive efficiency

$$\eta = kF_x U/(M_z \omega) \qquad (4)$$

The denominator in Equation 4 is taken as a measure of the torsional power required to drive the fin where M_z is the moment measured by the force sensor and ω (= $2\pi f$) is the circular frequency of flapping. k is a non-dimensional scaling constant.
Fig. 5 shows the variation of C_T over the four fin shapes of different materials (Delrin, Polyimide, and Polyethylene). C_T increased with frequency except for Shape S1 of Polyimide and Shape S2 of Polyethylene fins. These two fins have a drastic drop in C_T after a certain frequency and then it begins to increase again. One possible explanation for this is that the force generation at lower frequencies for these two fins is viscous drag dominant. This effect drops after the Reynolds number, contribution of added mass, and pressure drag start to increase. Fig. 6 shows the variation of η (measure of efficiency) with Strouhal number for all the fins used. The relatively more rigid Delrin fins have peak efficiencies in the range of 0.8-1. Polyimide fins do not have much variation, for most part, with Strouhal number. The low efficiency of the Polyethylene fins can once again be explained by high viscous drag.
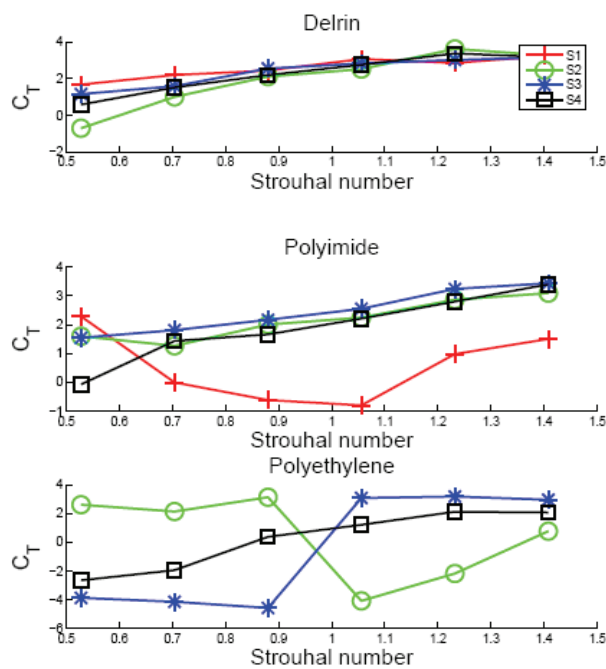
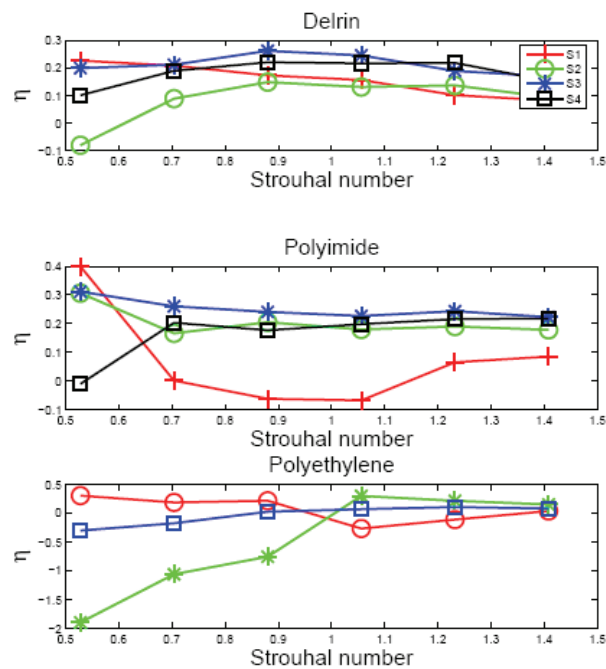Fig. 5. Variation of thrust coefficient with frequency.

Fig. 6. Variation of efficiency with frequency.

The criteria for fin selection should be high values for C_T and η over a range of frequencies. Caudal fin flapping frequency is one of the key parameters that has to be changed to control the speed of the MUV. Thus, a fin with good thrust production and high efficiency over a range of frequencies is desirable. Shape S3 of Polyimide clearly is the best choice as indicated by the C_T and η values.

3. Body stability

This study seeks to understand the role of different morphological parameters that could be responsible for boxfish stability and transform such findings into engineering design guidelines for the body shape design of a micro underwater vehicle. The analysis was performed using Computer Aided Design and Engineering (CAD/CAE) tools such as solid modeling software and fluid flow simulation software. First approximate models of boxfish were built in 3D modeling software and fluid flow was simulated over such models to analyze the vorticity patterns around the body. The relative role of key morphological features like the dorsal and ventral keels, concavity and convexity of the shape, and changes in the cross section along the length of the body were determined. Different MUV body shape designs were built along these lines and tested for required vortex strength and overall drag to arrive at the best design.

Fig. 7 shows the counter rotating vortex shedding by a bluff body. The vortex shedding should result in moments that can correct disturbances in the pitch and yaw(not shown in the Figure) directions. The shape that can demonstrate this 'selfcorrecting vortex shedding' for pitch and yaw disturbances will be the shape suitable for the body of the MUV.

The morphological features that contribute to the unique vortex shedding patterns as reported in (Bartol, et. al, 2005) had to be identified to be incorporated into the design. Approximate 3D models capturing essential features of the boxfish were made and flow at different angles of attack was simulated over such models to study the role of the various features on stability. SolidWorksR , a 3D CAD modeling software was used to build body shapes and fluid flow simulation was carried out using GAMBIT ™ (for defining boundaries of the flow and laying computational grid around the body) and FIDAP™ (for solving the flow and post processing) of FLUENT Inc.
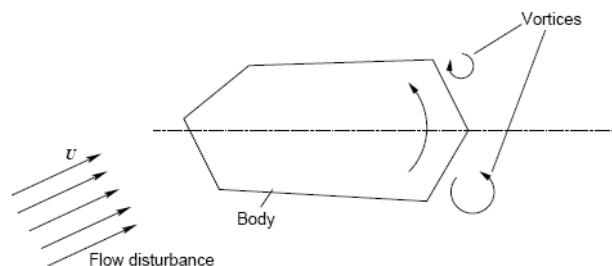

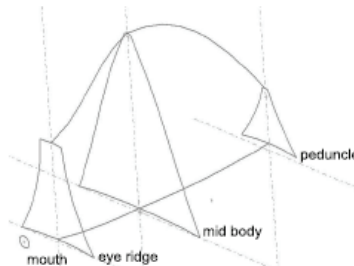Fig. 7. Self-correcting vortex shedding in boxfish body.

Fig. 7. Cross sections along the body of the buffalo trunk fish.

3D models of boxfish were built in SolidWorks. Essential features like dorsal and ventral keels and variation in cross sections along the length of the body were reproduced in the models. Variation of cross section along the body plays a very significant role in the vorticity

generation: therefore, cross sections near mouth, eye ridge, peduncle, and any other distinct plane were drawn on 2D planes and joined to obtain the desired shape. Fig.7 shows the planes containing important cross sections of the buffalo trunk fish. Only two, the Spotted boxfish and the Buffalo trunkfish, of the four varieties of boxfish studied in (Bartol, et. al, 2005) were considered here. The other two shapes are not significantly different from the buffalo trunkfish. Fig. 8(a) and 9(a) show the planar views of the actual boxfish used in the study by Bartol et. al. 3D models of the fish used in this study are shown in Fig. 8(b) and 9(b). It has to be noted that the 3D models were developed only based on subjective 'resemblance', capturing the key features and not accurate measurements of the boxfish morphology.

(a) Planar views of the Spotted boxfish considered by Bartol et al. in [11]
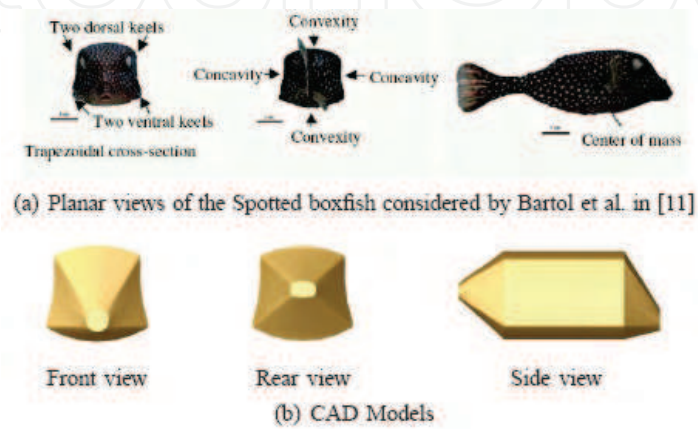
(b) CAD Models

Fig. 8. Spotted boxfish

Fig. 9. Buffalo trunkfish

Once created, the 3D models were imported into GAMBIT in IGES format. The imported models were then 'cleaned' by merging unwanted edges and surfaces that may have hindered mesh generation. To take advantage of the lateral symmetry of the boxfish shape, only (left/right) half of the body was considered for simulation. An external brick volume was used for the fluid flow. The symmetry plane of the boxfish was made coincident to one of the brick side walls and the body was placed midway along the height and length of the brick (see Fig. 15). In future simulations, the size of the brick could be increased further to minimize the wall effects. Fig. 15 shows the 3D mesh generated in GAMBIT. Shape functions have been defined such that the mesh is finer near the body surfaces and gets coarser away from the body. The mesh size was kept fairly coarse in order to keep the

convergence time reasonable. The course mesh was not detrimental to the simulation results because the Reynolds number was only about 300, and thus did not require a very dense mesh. It has to be noted that the Reynolds number corresponds to the case where a water wave disturbs an otherwise stationary boxfish and therefore is lower than the average Reynolds number of boxfish swimming.

Here the main results and conclusions are summarized and compared to those reported in (Bartol, et. al, 2005). First, it was reported in (Bartol, et. al, 2005)that the ventral keels of all the models produced Leading Edge Vortices (LEVs) that grew in circulation along the bodies, and this was verified in the present study. Vorticity concentration was found at the keel edges for all the models at various cross sections. Vorticity contours at different cross sections for both the fish can be found in (Kodati, 2006). This is expected, as the keels form the sharp corners of the body and hence induce circulation into the oncoming water. However, for a given angle of attack an increase in circulation was found only when there is a sudden increase in the cross section. This is true for both the boxfish shapes. For the spotted boxfish in Fig. 10, the maximum concentrated vorticity is located at the eye ridge, where the cross section increases suddenly. Similar behavior was observed for the Buffalo trunkfish. The concentrated vorticity near the keels increased along the length until it reached a maximum at the mid body plane, where the body curve attains a peak (Fig. 11).

Second, the present study also verified that vortices formed "above the keels and increased in circulation as pitch angle became more positive, and formed below the keels and increased in circulation as pitch angle became more negative", verbatim from (Bartol, et. al, 2005). Fig. 11 shows the net vertical lift on the spotted boxfish model varying with pitch angle. In (Bartol, et. al, 2005) the lift coefficients of all the boxfish studied were very near the origin (that is, almost no lift at zero angle of attack). The difference might be error due to the fact that the actual boxfish dimensions were not reproduced in the solid model.

Third, it was found that vortices formed along the eye ridges of all the boxfish: this was clear from the simulation - the eye ridge regions for both the models have shown concentrated vorticity, which once again can be attributed to the sudden increase in the cross section profile. Finally, when both boxfish were positioned at various yaw angles, regions of stronger concentrated vorticity formed in far-field locations of the carapace when compared with nearfield areas, and vortex circulation was greatest in the posterior of center of mass, just as described in (Bartol, et. al, 2005). The vorticity contours for the yaw case are not presented here for the sake of brevity and can be found in (Kodati, 2006).
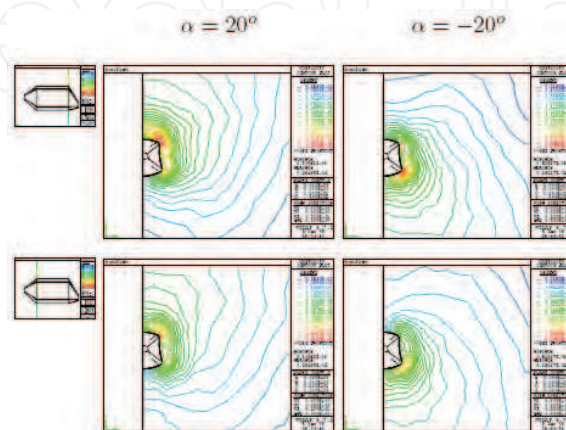

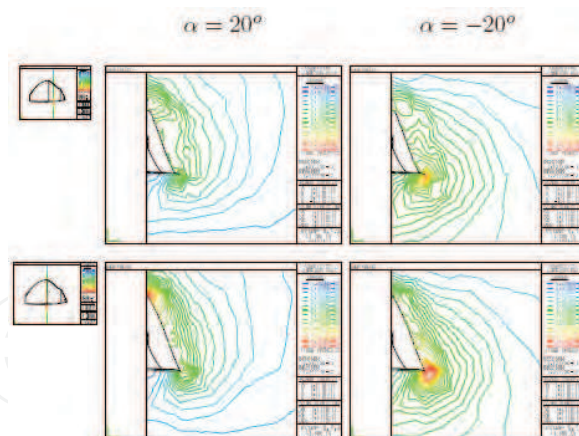Fig. 10. Vorticity countour maps at various cross sections of the spotted boxfish.

Fig. 11. Vorticity countour maps at various cross sections of the buffalo trunkfish.

From the analysis of the actual boxfish like shapes, it has been determined that the following two shape factors are mainly responsible for altering the vortex generating characteristics. First, change in the cross section profile: along the body for pitch stability and across the body for yaw stability. Second, sharpness of the keels that, in turn, depend on the concavity and convexity of the joining faces. These two characteristics were explored in the design of the MUV. Fig. 19 shows parameters used to change the body shape of the MUV. In order to verify the first of the two factors (cross section profile change), the shapes shown in Fig. 20 were considered. Both shapes were modified in the front region, and the rear change of area (the 'bump') was increased in the second shape. When flow was simulated at different pitch angles on both models, the peak vorticity was found to be higher for the second case at all angles of attack, as expected. The concavity of the side surfaces determines the sharpness of the keel and hence can affect the flow separation. To verify this, models with concave, flat, and convex surfaces were considered. There was not much variation in peak vorticity in the simulations for different pitch angles, but the vorticity was concentrated more heavily on the keels of the concave shape than on the flat and convex shapes. For yaw angles of attack, the peak vorticity was higher for the concave design and the vorticity was still concentrated near the keels. A comprehensive set of simulation results can be found in (Kodati, 2006).

4. Robotic prototype development

Boxfish employ a total of five fins to maneuver effectively. Biologists have observed three main swimming gaits employed at three different speed levels (Gordon, et. al, 2000). The design issue is how many of these fins can be practically implemented in a small underwater vehicle and how many degrees of freedom are used for each fin motion. For effective planar maneuverability, the degrees of freedom have to be distributed around the body. The present design incorporates a single DOF flexible tail fin for propulsion and a pair of 2 DOF pectoral fins for steering (yawing) and diving (pitching). Although the dorsal and anal fins of boxfish are believed to play a role in generating low recoil movement (Gordon, et. al, 2000), they are not included in the design due to size constraints.

The 2DOF pectoral fins use flapping and rotational motion in the so-called rowing mode. Rowing mode is a drag based thrust generation stroke with a full cycle of the fins. The power stroke is a quick backward push of the oil with the chord length perpendicular to the water flow. The recovery stroke involves bringing back the fin with the chord length parallel

to the flow. The rotation DOF is used to change the orientation of the fin at stroke reversals. This type of system can generate substantial turning moments about the body center of mass for sharp turns (Walker, 2000). The pectoral fins can also be used effectively as lifting surfaces by holding them at a suitable angle of attack to an oncoming flow.
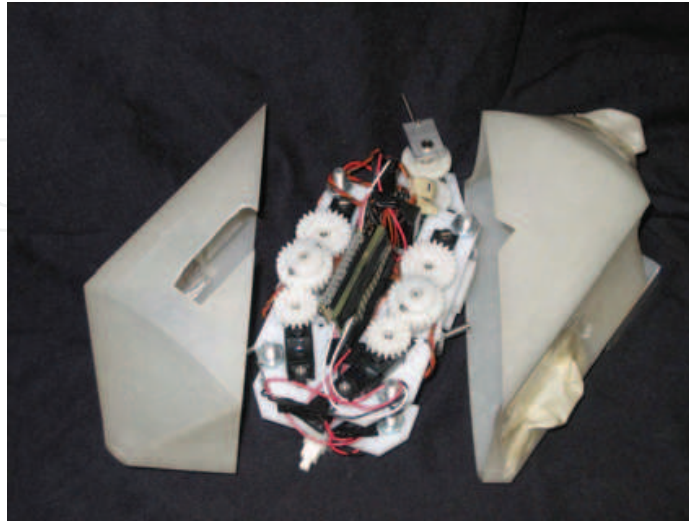

Fig. 12. Robotic prototype development.

A coaxial wrist mechanism has been designed that is similar to the robotic flapper design presented in (Kodati, 2007). The difference is that there is no deviation DOF and the gearbox size has been shrunk to a 2 cm × 2cm × 2cm volume using the smallest off-the-shelf miter gears available. The tail fin mechanism consists of a gear stage between the tail fin shaft and the motor shaft. The side fin flapping and rotation angles are coupled due to the no-slip condition of the wrist bevel gear box. A parallel plate structure was used to place the pectoral fin motors in front and above the wrist gear box. The electronic chips were placed on the top plate along with the pectoral fin motors and transmission mechanism. The battery pack, tail fin motor, and transmission were mounted on the bottom plate. The plates are made out of 0.125 inch thick Delrin sheet. A CNC mill was programmed to machine all the features on the plates.

Fig. 13. Swimming Experiments.

Accurate positioning of the fin flapping angles was required to control the force generation for turning and cruising. Servo motors with built in feedback were used in place of a DC motor and encoder combination. All the servos are daisy-chained to a servo controller that drives them to the position commanded by the processor. The onboard electronics include a Javelin-Stamp TMmicroprocessor module by Parallax Inc. and a serial motor controller PCB unit by Pololu Inc. The power supply for the motors, motor controller, and processor is provided by a pack of five 1.2V NiMH batteries. The microprocessor was programmed using an embedded Java version. A Java class routine was used to command the motor controller in serial communication mode using a built-in UART object.

The outer shape of the MUV was rapid prototyped using the stereolithograhy (3D printing) technique. Features for assembly and fin placement were incorporated into the shape. To seal the robot, layers of adhesive tape and oil resistant film were applied along the dividing line between the two body halves. The fin extensions were covered with latex sheet and attached to the shaft with a plastic O-ring. The latest configuration of the robot is one in which the body shape is assembled in diagonal halves as shown in Fig. 12. Fig. 13 shows the swimming prototype.

For the robot to be neutrally buoyant, the weight force must be equal to the buoyancy force. The buoyancy is determined by the volume of oil (experimental trials were conducted in a low viscosity, clear oil to avoid electrical shorting) displaced by the solid model. Copper bars, machined to fit underneath the chassis plates, were used to balance the buoyancy force and the weight force. The heaviest parts, such as the batteries and large copper plate, were designed to fit in the lower region of the robot. By placing the center of mass below the center of buoyancy, the robot was designed to have inherent stability. The location of the center of mass was found by hanging the prototype from a string attached at different points and taking an image. The images were overlaid on top of one another and a line was drawn to extend the line of the string. The approximate point of intersection of all the lines was the experimental center of mass.

The current robotic prototype can be programmed to use different gait styles. A CCD camera, by Allied Vision Technology, operating at 30 fps was used to record swimming trials and determine speed, recoil movement, and turning radius. The robot was run in the field of view of the camera and each image was saved in National Instrument's Vision Assistant for LabVIEW. A Virtual Instrument (VI) was created to calibrate the pixels to real world units of inches. Each image was then sequentially analyzed for the speed, recoil, and turning radius. The speed and turning radius were measured by the change in position of a point on the robot and a constant point ing the field of view. The average speed obtained was 0.0411 m/s with an almost zero turning radius. The recoil can be measured by the deviation in each frame from the straight line between the beginning and end points. The average recoil was found to be 0.826 cm. The gait used for the test is shown in Fig. 27. The green color of the fins indicates the phase of the stroke where forward propulsive thrust is produced, and the red color indicates the phase where the force generated is either minimal (like the recovery stroke of the pectoral fin) or in the direction opposite to the motion of the robot (as in the case of the caudal fin). The gait in Fig. 27 is one where a constant forward propulsive force is applied to the body during most of the caudal fin cycle.

5. Conclusion

In this chapter present the research leading to the design of a biologically inspired robotic boxfish using multiple fins. The design attempts to achieve the maneuverability of a small scale, multiple fin underwater system like that of the boxfish, while also incorporating a body with a self correcting mechanism.

Experimental studies were conducted to characterize and optimize the flapping fin propulsion of the tail fin. Towards this a three DOF robotic flapper was designed to act as the flapping tail or side fin of the fish and a fixed beam based force sensor was designed to measure the instantaneous forces generated by the fin motion. Tail fin with optimal shape induced flexibility has been found. The hydrodynamic force generation of tail fin has been modeled using a combination of quasi steady lift generation and empirically found drag and added mass effects. Fluid flow simulations on 3D CAD models of boxfish like shapes were used to arrive at the outer shape of the MUV. A robotic prototype of the MUV was designed based on the above analysis. The propulsion and maneuvering of the MUV is achieved by tail fin and two 2DOF side fins.

One of the immediate goals is to use the prototype to evaluate the efficiency of various gait patterns for a given set of flow conditions. Sensors and command architecture will also be used in future generations to give the robot greater autonomy. Currently, new mechanical sealing techniques and more processing power are being incorporated into the next generation of the prototype to facilitate longer trial runs and effective control of the robot. Studying fin-fin and body-fin interactions can help modify the design of body shape and/or fin kinematics for optimal thrust production or even better maneuverability. One such problem is that of the interaction between the side fin and tail fin. On a small robot like the present MUV the proximity of the side fin and the tail fin is more and can lead to strong interactions between them. Such mechanisms can be investigated using multiple flappers and/or body shape in the tow tank.

6. References

Bandyopadhyay, P. (2005) Trends in biorobotic autonomous undersea vehicles," IEEE Journal Of Oceanic Engineering, vol. 30, no. 1, January 2005.

Barrett, D.; Triantafyllou, M.; Yue, D.; Grosenbaugh, M. & Wolfgang, M. (1999) Drag reduction in fish-like locomotion," *Journal of Fluid Mechanics*, vol. 392, pp. 183–212, 1999.

Bartol, I.; Gharib, M.; Webb, P.; Weihs, D. & Gordon, M. (2005) Body-induced vortical flows: a common mechanism for self-corrective trimming control in boxfishes," *Journal of Experimental Biology*, vol. 208, pp. 327–344, 2005.

Breder, C. (1926) The locomotion of fishes, *Zoologica*, vol. 4, pp. 159–256, 1926.

Colgate, J. & Lynch, K. (2004) Mechanics and control of swimming: A review, *IEEE Journal of Oceanic Engineering*, vol. 29, no. 3, July, 2004.

Combes S. & Daniel, T. (2003) Flexural stiffness in insect wings. II. spatial distribution and dynamic wing bending." *Journal of Experimental Biology*, vol. 206, no. 17, 2003.

Epstein, M.; Colgate, J. & MacIver, M. (2006) Generating thrust with a biologically-inspired robotic ribbon fin," in *Proc. of IEEE/RSJ Int. Conf. on Intelligent Robots and Systems (IROS)*, Beijing, China, 2006.

Fish, F.; Lauder, G.; Mittal, R.; Techet, A.; Triantafyllou, M.; Walker, J. & Webb, P. (2003) Conceptual design for the construction of a biorobotic auv based on biological hydrodynamics. *In Proceedings of the 13th international symposium on Unmanned Untethered Submersible Technology*, 2003.

Floyd, J.; Keegan T. & Sitti, M. (2006) A novel water running robot inspired by basilisk lizards," in *Proc. of IEEE/RSJ Int. Conf. On Intelligent Robots and Systems (IROS)*, October 2006.

Gordon, M.; Hove, J.; Webb, P. & Weihs, D. (2000) Boxfishes as unusually well-controlled autonomous underwater vehicles," *Physiol. Biochem. Zool.*, vol. 74, no. 6, pp. 663–671, 2000.

Kato,B. & Wicaksono, N. (2000) Development of biology-inspired autonomous underwater vehicle bass iii with high maneuverability," in *Proceedings of the 2000 International Symposium on Underwater Technology*, pp. 84–89, 2000.

Kodati, P. (2006) Biomimetic micro underwater vehicle with ostraciiform locomotion: System design, analysis and experiments, Master's thesis, University of Delaware, Newark, DE, USA, August 2006.

Kodati P. & Deng, X. (2007) Experimental studies on the hydrodynamics of a robotic ostraciiform tail fin," in *Proc. of IEEE/RSJ Int. Conf. On Intelligent Robots and Systems (IROS)*, October 2006, pp. 5418–5423.

Lachat, D.; Crespi, A. & Ijspeert, A. (2006) Boxybot: a swimming and crawling fish robot controlled by a central pattern generator," in *Proceedings of The first IEEE / RAS-EMBS International Conference on Biomedical Robotics and Biomechatronics*, 2006,

Licht, S.; Polidoro, V.; Flores, M.; Hover, S. & Triantafyllou, M. (2004) Design and projected performance of a flapping foil auv," *IEEE Journal of Oceanic Engineering*, vol. 29, no. 3, 2004.

Liao, G.; Beal D. & Triantafyllou, M. (2003) Fish exploiting vortices decrease muscle activity," *Science*, vol. 302, pp. 1566–1569, 2003.

Lindsey, C. (1978) Form, function and locomotory habits in fish, *Fish Physiology Volume VII: Locomotion*, W. S. Hoar and D. J. Randall, Eds. New York: Academic, 1978, pp. 1–100, 1978.

MacIver, M.; Fontaine, E. & Burdick, J. (2004) Designing future underwater vehicles: Principles and mechanisms of the weakly electric fish," *IEEE Journal of Oceanic Engineering*, vol. 29, no. 3, July 2004.

McIsaac K. & Ostrowski, J. (2003) Motion planning for anguilliform locomotion, *IEEE Transactions on Robotics and Automation*, vol. 19, no. 4, August 2003.

Mohseni, K. (2004) Zero-mass pulsatile jets for unmanned underwater vehicle maneuvering, in *AIAA 3rd "Unmanned Unlimited" Technical Conference, Workshop and Exhibit*, Chicago, IL, September 2004.

Sfakiotakis, M.; Lane, D. & Davies, J. (1999) Review of fish swimming modes for aquatic locomotion, *IEEE Journal of Oceanic Engineering*, vol. 24, no. 2, April 1999.

Triantafyllou, M. & Triantafyllou, G. (1995) An efficient swimming machine, *Scientific American*, vol. 272, no. 3, 1995.

Walker, J. (2000) Does a rigid body limit manuerability?, *Journal of Experimental Biology*, vol. 203, pp. 3391–3396, 2000.

Yuh, J. (2000) Design and control of autonomous underwater robots: A survey," *Autonomous Robots*, vol. 8, pp. 7–24, 2000.

Zhu, Q.; Wolfgang, M.; Yue, D. & Triantafyllou, M. (2002) Threedimensional flow structures and vorticity control in fish-like swimming, *Journal of Fluid Mechanics*, vol. 468, pp. 1–28, October 2002.

Underwater Vehicles

Edited by Alexander V. Inzartsev

For the latest twenty to thirty years, a significant number of AUVs has been created for the solving of wide spectrum of scientific and applied tasks of ocean development and research. For the short time period the AUVs have shown the efficiency at performance of complex search and inspection works and opened a number of new important applications. Initially the information about AUVs had mainly review-advertising character but now more attention is paid to practical achievements, problems and systems technologies. AUVs are losing their prototype status and have become a fully operational, reliable and effective tool and modern multi-purpose AUVs represent the new class of underwater robotic objects with inherent tasks and practical applications, particular features of technology, systems structure and functional properties.

How to reference

In order to correctly reference this scholarly work, feel free to copy and paste the following:

Parasar Kodati and Xinyan Deng (2009). Bio-inspired Robotic Fish with Multiple Fins, Underwater Vehicles, Alexander V. Inzartsev (Ed.), ISBN: 978-953-7619-49-7, InTech, Available from: http://www.intechopen.com/books/underwater_vehicles/bio-inspired_robotic_fish_with_multiple_fins

INTECH
open science | open minds